Synthesis, structure elucidation and redox properties of ^{99}Tc complexes of lacunary Wells Dawson polyoxometalates: insights into molecular ^{99}Tc – metal oxide interactions

Donna McGregor[#a,b]*, Benjamin P. Burton-Pye*[#a]*, Robertha C. Howell*[a,]*, Israel M. Mbomekalle*[a,c]*,*
Wayne W. Lukens, Jr.[d]*, Fang Bian*[a,b]*, Edward Mausolf*[e]*, Frederic Poineau*[e]*, Kenneth R Czerwinski*[e]*,*
and Lynn C. Francesconi[a,b*]

[#]*Contributed equally to this work*

[a]Hunter College of the City University of New York

695 Park Avenue, New York, NY 10065

[b] Graduate Center of the City University of New York New York, NY 10016

[d]Chemical Sciences Division, The Glenn T. Seaborg Center, E.O. Lawrence Berkeley National Laboratory (LBNL), One Cyclotron Road, Berkeley, CA 94720

[e]Department of Chemistry, University of Nevada Las Vegas, Las Vegas, NV 89154, USA

[c]present address: Institut Lavoisier, UMR8180, Université de Versailles St. Quentin, 45 Avenue des Etats-Unis, 78035 Versailles Cedex, France

[*]Email: lfrances@hunter.cuny.edu

ABSTRACT

The isotope ^{99}Tc (β_{max}: 250 keV, half-life: 2 x 10^5 year) is an abundant product of uranium-235 fission in nuclear reactors and is present throughout the radioactive waste stored in underground tanks at

Hanford and Savannah River. Understanding and controlling the extensive redox chemistry of ^{99}Tc is important to identify tunable strategies to separate ^{99}Tc from spent fuel and from waste tanks and once separated, to identify and develop an appropriately stable waste-form for ^{99}Tc. Polyoxometalates (POMs), nanometer sized models for metal oxide solid-state materials, are used in this study to provide a molecular level understanding of the speciation and redox chemistry of incorporated ^{99}Tc. In this study, ^{99}Tc complexes of the $(\alpha_2\text{-}P_2W_{17}O_{61})^{10-}$ and $(\alpha_1\text{-}P_2W_{17}O_{61})^{10-}$ isomers were prepared. Ethylene glycol was used as a "transfer ligand" to minimize the formation of $TcO_2 \bullet xH_2O$. The solution structures, formulations, and purity of $Tc^VO(\alpha_1/\alpha_2\text{-}P_2W_{17}O_{61})^{7-}$ were determined by multinuclear NMR. X-ray Absorption Spectroscopy of the complexes are in agreement with the formulation and structures determined from ^{31}P and ^{183}W NMR. Preliminary electrochemistry results are consistent with the EXAFS results, showing a facile reduction of the $Tc^VO(\alpha_1\text{-}P_2W_{17}O_{61})^{7-}$ species compared to the $Tc^VO(\alpha_2\text{-}P_2W_{17}O_{61})^{7-}$ analog. The α_1- defect is unique in that a basic oxygen atom is positioned toward the α_1- site and the Tc^VO center appears to form a dative metal-metal bond with a framework W site. These attributes may lead to the assistance of protonation events that facilitate reduction. Electrochemistry comparison shows that the Re^V analogs are about 200 mV more difficult to reduce in accordance with periodic trends.

INTRODUCTION

The isotope ^{99}Tc (β_{max}: 293.7 keV, half-life: 2.1 x 10^5 year) is of interest and concern for two reasons: 1) ^{99}Tc is a major product of uranium-235 fission in nuclear reactors ($\sim$ 6% thermal neutron fission yield) and 2) large amounts of ^{99}Tc, formed during early plutonium production activities, are present in the radioactive waste stored in underground tanks at Hanford and Savannah River. [1,2]

The physical properties of ^{99}Tc and its complex redox activity pose a problem for both closing the nuclear fuel cycle and remediation of waste tanks. In a storage repository, the long half-life of ^{99}Tc means that its waste form must be resistant to degradation. Understanding and controlling the extensive redox chemistry of Tc is important in identifying strategies to separate it from the tank waste and spent nuclear fuel, and are important in identification and development of an appropriately stable waste-form for ^{99}Tc once separated from spent nuclear fuel and from waste tanks.

The interplay between the specific oxidation state of ^{99}Tc and the "ligands" present in the tank waste or the coordination environment in a specific storage material determines the speciation and stability of the Tc within those materials. One crucial gap in the knowledge that needs to be filled to address both separation from tank waste and design of storage matrices is a molecular level understanding of the factors that control the oxidation state of 99Tc in metal-oxide matrices. In nuclear waste and in aerobic environments, the most stable Tc oxidation state is Tc(VII), which is highly environmentally mobile and generally not appropriate for disposal in a waste repository. In most existing and proposed waste forms, the desired oxidation state is Tc(IV) since Tc(IV) is not environmentally mobile and since the ionic radius of Tc(IV) is similar to that of Ti(IV) and Fe(III), which may allow Tc(IV) to be incorporated into the lattices of titanium or iron oxides. (refs: Langton, C. A. Challenging Applications for Hydrated andChemically Reacted *Ceramics*; DP-MS -88-163; Savannah River Laboratory: Aiken, SC, 1988. Khalil, M.Y.; White, W.B. *J. Amer. Ceram. Soc.***1983**, *66*, C-197. Singh, D.;, Mandalika˴ V.R.;, Parulekar˴ S.J.;Wagh˴ A.S. *J. Nucl. Mat.* **2006**, *348*, 272.)

Polyoxometalates (POMs) are soluble nanometer sized models for metal oxide solid-state materials.[3-5] We postulate that POMs, polyanionic aggregates of early transition metals (Mo^{VI} and W^{VI}), may provide an understanding of the coordination chemistry, oxidation state and speciation of ^{99}Tc incorporated into metal oxides. Oxygen atoms of the plenary structures are close packed, simulating solid oxide structures. The surface basicity of the POM structure can be altered by replacement of a lower valent ion for M^{VI} (M=Mo, W). Polyoxometalates possess alternating bond order differences resulting in rings exhibiting alternating short-long O-M-O bonds.[6] Binding of counterions and protonation dynamics of the POMs may be analogous to the dynamics found in solid-state metal oxide materials.

The defects of POMs possess specific and distinct steric and electronic features that can affect coordination chemistry and impact redox stability of technetium. Specifically, in this study, mono-vacant defect structures of the Wells-Dawson ion ((α_2-$P_2W_{17}O_{61}$)$^{10-}$ and (α_1-$P_2W_{17}O_{61}$)$^{10-}$ isomers) possess defects with clearly different steric and electronic properties, **Figure 1**. These α_1 and α_2 defects have different redox properties and binding strength to transition metals. Studies on lanthanide and transition metal POM speciation support the notion that the high basicity of the α_1 vacancy requires high charge/size cations for stabilization.[7-18] The elevated basicity of the α_1 defect is ascribed by Contant[9] to the orientation of the PO_4^{3-} tetrahedron within the cavity of the W-O framework, positioning a basic oxygen atom near the α_1 site. Transition metal cations substituted into the α_1 (belt) position are more readily reduced than when substituted in the α_2 (cap) position.[10,12,14,19,20]

In this study, ^{99}Tc complexes of the (α_2-$P_2W_{17}O_{61}$)$^{10-}$ and (α_1-$P_2W_{17}O_{61}$)$^{10-}$ isomers are prepared, characterized by multinuclear NMR, X-ray Absorption Spectroscopy and preliminary electrochemical studies are reported. The reduction and oxidation of Tc^V is compared in these isomeric complexes

along with the reduction and oxidation of the Re^V analogs. We attempt to identify the features of the polyoxometalate that impact reduction potentials of technetium.

Key prior studies of related Tc and Re POMs. Rhenium, Re, the third row congener of Tc, has been used as a non-radioactive surrogate for Tc. Re possesses higher reduction potentials, slower kinetics and often an expanded coordination sphere compared with Tc[21-23] and should be used with caution as a Tc substitute.

The $(Re^VO)^{3+}$ and $(Tc^VO)^{3+}$ units have been introduced into the lacunary α-Keggin, α-$XW_{11}O_{39}^{n-}$ (X=P, n=7; X=Si, n=8).[24,25] The purity of these analogs has been demonstrated by IR, electrochemistry, mass spectrometry and EPR (Re^{VI}). We have isolated pure $Re^{V, VI, VII}$ (α2-$P_2W_{17}O_{61})^{10-}$ complexes as verified by ^{31}P and ^{183}W NMR spectroscopy along with the above mentioned techniques.[26] A slight modification of crystallization using acidic conditions of the aqueous Re^VO-α2-$P_2W_{17}O_{61}$ complex resulted in a 2:2 dimer.[27]

EXPERIMENTAL SECTION

General. All materials were purchased as reagent grade and used without further purification. Potassium hexachlororhenate was purchased from Aldrich (99.99% purity). ^{99}Tc is a weak β- emitter with a half-life of 2×10^5 years. All syntheses and sample preparations were performed in laboratories approved for low-level use of radioactivity using appropriate radioactive material handling procedures. $^{99}TcO_4^-$ was purchased as the ammonium salt from Oak Ridge National Laboratory and treated with H_2O_2 to oxidize any reduced Tc.[28] $(NBu_4)TcOCl_4$ was prepared from NH_4TcO_4 according to an established procedure.[29] $K_9Li(α_1-P_2W_{17}O_{61})$ **(α1)** and $K_{10}(α_2-P_2W_{17}O_{61})$ **(α2)** ligands were prepared as described in the literature.[9,30] The preparation of $α_1-[Fe(H_2O)P_2W_{17}O_{61}]^{7-}$ **(Fe-α1)** and $K_{7-n}H_n[Re^VO(α_2-P_2W_{17}O_{61})]$ **(Re^VO-α2)** for electrochemistry were described previously.[26,30] Analytical grade CH_3COONa (Fisher) and glacial CH_3COOH (Acros) were used as received. Centrifugations were

performed with an International Equipment Co. Model CL Clinical centrifuge. Pure water used throughout was obtained using a Millipore Direct Q5 system (conductivity =18 $\mu\Omega$). Infrared analyses were performed on a Perkin Elmer 1625 FTIR Spectrometer. Negative-ion electrospray mass spectra were recorded on a VG Quattro at the University of Illinois School of Chemical Sciences Mass Spectrometry Resource.

Collection of NMR Data. NMR data were collected on a JEOL GX-400 spectrometer with 5 or 10 mm tubes fitted with Teflon insert that were purchased from Wilmad Glass. Resonance frequencies are 161.8 MHz for ^{31}P and 16.7 for ^{183}W. Chemical shifts are given with respect to external 85% H_3PO_4 for ^{31}P and 2.0 M Na_2WO_4 for ^{183}W. Typical acquisition parameters for ^{31}P spectra included the following: spectral width, 10000 Hz; acquisition time, 0.8 s; pulse delay, 1 s; pulse width, 15 μs (50° tip angle). From 200 to 1000 scans were required. For ^{183}W spectra, typical conditions included the following: spectral width, 10000 Hz; acquisition time, 1.6 s; pulse delay, 0.5 s; pulse width, 50 μs (45° tip angle). From 1000 to 30000 scans were acquired. For all spectra, the temperature was controlled to $\pm$ 0.2 deg. For the ^{31}P and ^{183}W chemical shifts, the convention used is that the more negative chemical shifts denote more upfield resonances.

Extended X-ray Absorption Fine Structure (EXAFS) Spectroscopy: Samples were dissolved in 1 mL of 18 MΩ water then transferred to 2 mL screw capped, polypropylene centrifuge tubes, which where sealed inside two, nested polyethylene bags. Using these samples, data was acquired at room temperature in transmission using Ar-filled ion chanbers at SSRL beamlines 11-2 and 4-1; data was collected using the locally written program XAScollect. Harmonic content of the beam was reduced by detuning the monochromator by 50%. The data was processed using EXAFSPAK and Athena/ifeffit.[31,32] Data was fit using Artemis/ifeffit and theoretical phases and amplitudes calculated using FEFF7.[33] The initial model used in the FEFF calculation was $(NH_4)_6(P_2W_{18}O_{62})$ with one W atom

replaced by Tc.[34] Additional scattering shells were added only if their inclusion lowered the value of reduced chi squared.

The F-test was used to analyze the significance of the fitting parameters including the significance of adding a scattering shell.[35] The null hypothesis is that the additional shell of atoms does not improve the fit. The result of the F-test is the probability, p, that this hypothesis is correct. If $p < 0.05$, the null hypothesis is rejected in favor of the alternative hypothesis that the additional shell significantly improves the fit.[36]

Electrochemical Data Collection: Electrochemical data were obtained using a BAS Voltammetric Analyzer System controlled by BAS CV-50W software (for PC). The cell used for cyclic voltammetry (CV) contained a glassy-carbon working electrode (BAS standard disk electrode, 3 mm OD), a Pt wire auxiliary electrode (0.5 mm), and a BAS Ag/AgCl (3 M NaCl), reference electrode.

Electrochemistry of the compounds were conducted at a concentration of 0.2 mM in pH 5 buffer (0.5 M $NaSO_4$ in 0.01 M NaOAc). Prior to obtaining electrochemical data, solutions were de-aerated for at least 30 min with high purity Ar. A positive pressure of this gas was maintained during subsequent work. Preparation, including fine polishing of the glassy-carbon working electrode was adapted from the procedure of Keita and co-workers[37]. Unless indicated otherwise, scan rates were 10 mVs^{-1}, and all experiments were carried out at ambient temperature under an atmosphere of Ar.

Synthesis of compounds.

$\mathbf{K_{7-n}H_n[Tc^VO(\alpha_1\text{-}P_2W_{17}O_{61})]}$ **($\mathbf{Tc^VO\text{-}\alpha1}$):** To a 20 mL scintillation vial containing a yellow/green solution of $(NBu_4)TcOCl_4$ (100 mg, 0.2 mmol) dissolved in 1 mL MeOH was added 60 μL (0.98 mmol) of ethylene glycol $(CH_2OH)_2$ (eg) to produce a blue/green $TcO(eg)_2^-$ complex. This solution was quickly added to a clear, colorless solution of **α1** (447 mg, 0.099 mmol) dissolved in 5 mL H_2O containing LiCl (10 mg, 0.2 mmol). The resulting dark red solution and brown suspension was stirred

for 3 minutes. The reaction mixture was centrifuged (15 min 70,000 rpm) and the red supernatant decanted. KCl (0.16 g, 2 mmol) was added to the supernatant and was stored at room temperature for up to 48 hours to allow any unreacted **α1** (as monitored by ^{31}P NMR) to precipitate. The mixture exhibiting a clean, two peak ^{31}P NMR, was filtered and 20 mL of ethanol added to the filtrate to precipitate a dark red solid, which was collected by vacuum filtration.

Yield: 40 - 60% based on (NBu$_4$)TcOCl$_4$. IR (KBr, cm^{-1}): 790 cm^{-1} (strong, broad), 953 cm^{-1} (weak), 1086 cm^{-1} (strong).

K$_{7-n}$H$_n$[Tc^{V}O(α$_2$-P$_2$W$_{17}$O$_{61}$)] (Tc^{V}O-α2): To a 20 mL scintillation vial containing a yellow/green solution of (NBu$_4$)TcOCl$_4$ (100 mg, 0.2 mmol) dissolved in 1 mL MeOH was added 60 μL (0.98 mmol) of ethylene glycol to produce a blue/green TcO(eg)$_2^-$ complex. This solution was added quickly to a clear, colorless solution of **α2** (447 mg, 0.099 mmol) dissolved in 5 mL H$_2$O at 80 °C. The resulting dark red solution and brown suspension was stirred for 3 minutes. While still warm, the reaction mixture was centrifuged (15 mins, 70,000 rpm), the dark red supernatant decanted and KCl (0.16 g, 2 mmol) added. The red solution was allowed to sit at room temperature for up to 72 hours to allow any unreacted **α2** (as monitored by ^{31}P NMR) to precipitate. The mixture exhibiting a clean, two peak ^{31}P NMR, was filtered and 10 mL of ethanol was added to the filtrate to precipitate a dark red solid, which was collected by vacuum filtration.

Yield: 40 - 60% based on (NBu$_4$)TcOCl$_4$. IR (KBr, cm^{-1}): 790 cm^{-1} (strong, broad), 953 cm^{-1} (weak), 1086 cm^{-1} (strong).

K$_{7-n}$H$_n$[Re^{V}O(α$_1$-P$_2$W$_{17}$O$_{61}$)] (Re^{V}O-α1): A 200 mL round bottom flask was charged with K$_2$ReCl$_6$ (0.285 g, 0.6 mmol) and **α1** (2.39 g, 0.48 mmol), and deoxygenated water was added (30 mL) to form a slurry. The slurry was heated at 40 °C for 30 minutes producing a navy blue solution. The solution was cooled to room temperature, 125 mL of ethanol added, and the sample placed in the freezer

for 10 minutes. The dark microcrystalline solid was isolated by filtration and recrystallized twice from 50 mL hot water. The product was 95% pure as judged by ^{31}P NMR; Yield (1.08 g, 0.22 mmol). In order to remove impurities arising from the **Re^{V}O-α2** congener, 0.4 g of recrystallized product was dissolved in 5 mL distilled water and loaded onto a silica column (5.5 cm (diameter) x 60 cm filled to a height of 40 cm with silica) primed with methanol, and eluted with methanol. The dark blue fraction containing **Re^{V}O-α1** was reduced in volume by rotary evaporation and filtered to remove any silica. The solvent was then removed by rotary evaporation to yield pure **Re^{V}O-α1**, free from **Re^{V}O-α2**.

^{31}P NMR and the ^{183}W NMR data for the complexes are given in **Table 1**.

RESULTS AND DISCUSSION

Synthesis of Complexes. The synthesis of pure transition metal polyoxometalates is often complicated by the difficulty in separating unreacted POM ligand from the metal POM complex. Usually separations are achieved by fractional crystallizations and are complicated by the similar solubilities of the metal complexes of POMs and the POM ligands. Separations are rendered even more difficult due to the small volumes manipulated in fractional crystallizations when working with milligram quantities of ^{99}Tc. The small volumes, multiple oxidation states accessible to ^{99}Tc, and hydrolysis of the ^{99}TcOCl$_4^-$ starting reagent generally compromises separation of reactant from products, reproducibility and yield of the reactions

The (NBu$_4$)TcOCl$_4$ starting reagent readily hydrolyzes in water and in methanol; in order to stabilize this source of Tc^{V}O, (NBu$_4$)TcOCl$_4$ was treated with ethylene glycol, which acts as a "transfer ligand"[38] to inhibit hydrolysis of TcOCl$_4^-$ and facilitate transfer of Tc for isolation of **Tc^{V}O-α1** and **Tc^{V}O-α2**. The TcO(eg)$_2^-$ complex[39] was formed *in situ,* and the ethylene glycol ligands were replaced by the tetradentate **α1/α2** ligands to form the Tc^V complexes.

If too little ethylene glycol is used to stabilize Tc(V), hydrolysis of the $TcOCl_4^-$ starting material to $TcO_2 \bullet H_2O$ occurs, *vide infra*, resulting in inconsistencies in the ^{31}P NMR data used to monitor the progress of the reaction. The ^{31}P NMR resonances are often paragmagnetically broadened or not visible due to the presence of $TcO_2 \bullet H_2O$. $TcO_2 \bullet H_2O$ is typically colloidal and often cannot be filtered from the reaction solution. **Table S1** presents the ^{31}P NMR data for the stages of one such reaction.

In general, the crude reaction mix showed no peaks in the ^{31}P NMR (due to the presence of the paramagnetic $TcO_2 \bullet xH_2O$ species). The colloidal $TcO_2 \bullet xH_2O$ was removed from the crude reaction mixture by centrifugation. After centrifugation for 15 minutes at 70,00 rpm, the supernatant showed peaks of the desired product as well as excess **α1/α2** starting material. Allowing the supernatant to stand at room temperature overnight resulted in the precipitation of a mixture of white and black-brown material. The white solid was identified as the **α1** or **α2** ligand (by ^{31}P NMR), and the black-brown solid was postulated as a mixture of $TcO_2 \bullet xH_2O$ and **Tc^{V}O-α1** or **Tc^{V}O-α2** as a tetrabutylammonium salt (soluble in acetonitrile and identified by ^{31}P NMR).

After filtering to remove the solids, the dark red filtrate showed ^{31}P NMR peaks of pure product (**Table S1** shows this for **Tc^{V}O-α2**), further affirming that the white solid was indeed unreacted ligand. If the original supernatant was allowed to stand for periods more than one week $(\alpha-P_2W_{18}O_{62})^{6-}$ (the parent Wells-Dawson POM) formed in solution. This $(\alpha-P_2W_{18}O_{62})^{6-}$ was consistently difficult to separate from the desired product.

Isolation of solid product was initially attempted by adding an excess of KCl. Although this did result in the formation of a dark brown solid, once dissolved, this solid showed no identifiable product peaks in the ^{31}P NMR. In subsequent reactions, it was discovered that the use of a minor amount of KCl (to aid the precipitation of impurities and excess ligand), followed by the addition of an excess of ethanol resulted in the isolation of pure **Tc^{V}O-α1** or **Tc^{V}O-α2**, as identified by ^{31}P NMR. The yields obtained for these reactions were never more than 60 %. The low yields are primarily attributed to the

formation of $TcO_2 \cdot xH_2O$. It was found that maintaining a 1:1 ratio of Tc to **α1** or **α2** is important for optimizing the yield of product (albeit at ~ 50 %).

Even a small excess of Tc (>1 eq.) results in the formation of a large amount of dark brown/black precipitate (presumed to be $TcO_2 \cdot xH_2O$). Using an excess of **α1** or **α2** to compensate for this does not prevent formation of $TcO_2 \cdot xH_2O$; rather, the result is always an excess of **α1** or **α2** present in the crude product (as determined by ^{31}P NMR). This phenomenon would indicate that the formation kinetics of **Tc^VO-α1** or **Tc^VO-α2** are slower than that of the disproportionation of Tc(V) to $TcO_2 \cdot xH_2O$.

The use of ethylene glycol as a transfer ligand to inhibit the hydrolysis of $TcOCl_4^-$ and facilitate transfer of Tc for isolation of **Tc^VO-α1** and **Tc^VO-α2** proved successful. The $TcO(eg)_2^-$ complex[39] was not isolated during the procedure, but rather formed *in situ*. When **α1/α2** is added to this $TcO(eg)_2^-$ complex, the ethylene glycol ligands are replaced by the tetradentate **α1/α2** to form **Tc^VO-α1/α2**.

In addition to the 1:1 Tc: **α1** and **α2** stoichiometry, we found that a Tc:eg ratio of between 1:3.5 and 1:6 was required to obtain an optimal yield and purity. A ratio of less than 1:3.5 resulted in the formation of an increased amount of both the containing dark solid and free **α1** or **α2**, ligand, while a ratio of more than 1:6 resulted in a low yield and increased difficulty when isolating a pure product as a solid. It should be noted however, that upon scale-up of the reaction an increased ratio of eg:Tc became necessary to stabilize the Tc(V)O core from hydrolysis to $TcO_2 \cdot H_2O$.

Re^VO-α1 was initially prepared in the same fashion as reported for **Re^VO-α2** however, the preparation resulted in the formation of the parent Wells-Dawson ion, $(\alpha\text{-}P_2W_{18}O_{62})^{6-}$ and **Re^VO-α2** impurities. Elevated temperatures increased the amount of $P_2W_{18}O_{62}^{6-}$ and **Re^VO-α2**. Running the reaction at lower temperatures reduced the amount of P_2W_{18} and **Re^VO-α2** but did not eliminate the formation of these impurities entirely. Multiple recrystalizations were attempted to isolate pure **Re^VO-α1** but trace amounts of the **Re^VO-α2** isomer were visible by ^{31}P NMR. Column chromatography

utilizing silica gel as the stationary phase and employing methanol as eluent, separated the $Re^VO-\alpha2$ from $Re^VO-\alpha1$. **Figure S1** illustrates the purification process as monitored by ^{31}P NMR and cyclic voltammetry.

Characterization of Complexes:

Infrared Spectroscopy.

The infrared spectra of $Tc^VO-\alpha1$ and $Tc^VO-\alpha2$ show characteristic stretches at 790 cm^{-1} (strong, broad), 907 cm^{-1}, 953 cm^{-1} (weak), 1086 cm^{-1}(strong). Representative IR spectra (KBr pellet) are shown in the supporting material, **Figure S2**. The IR spectra are, not surprisingly, similar to the parent $(P_2W_{18}O_{62})^{6-}$. In a study by Ortega and Pope, the IR spectra for Re^V, Re^{VI}, Re^{VII} substituted into the $XW_{11}O_{39}^{n-}$ framework are similar to the parent $XW_{12}O_{40}^{(n+2)-}$.[25] We observed also, that the IR spectra for Re^V, Re^{VI}, Re^{VII} substituted into the $(\alpha_2-P_2W_{17}O_{61})^{10-}$ framework are similar to the parent $(P_2W_{18}O_{62})^{6-}$.[26] The Tc=O stretch is expected to occur at 900 – 960 cm^{-1} and that would overlap with the bands observed in the W framework.

Mass Spectrometry.

Negative-ion electrospray mass spectrometry provides data with minimal fragmentation and has been found to be a useful tool for the analysis of polyoxometalates.[8,26,40,41] The data for the mass spectrometry analysis of $Tc^VO-\alpha1$ and $Tc^VO-\alpha2$ are presented in **Table 2**. The highly negatively charged molecules form adducts with cations and thus different charge states can be formed. In aqueous solution, the 4⁻, 3⁻ and 2⁻ charge state clusters are observed. **Table 2** and **Figure S3** show the corresponding m/z values for the various charge states of the molecules with variable amounts of potassium and proton adducts. Taken with the multinuclear NMR data, *vide infra*, these mass spectral data confirm the formulation of the technetium complexes.

Multinuclear NMR Spectroscopy. Multinuclear NMR spectroscopy, given in **Table 1**, is used to establish the purity and structure of **Tc^{V}O-α1**, **Tc^{V}O-α2** and **Re^{V}O-α1**. ^{31}P NMR is a well-established technique to assess impurities of polyoxometalates at the 2% level [42-44] and has been used to identify pure Wells-Dawson complexes of transition metals[42-46] and lanthanides[8,16-18,45,47-52]. (We also turn to electrochemistry to clearly observe signature patterns that identify the **α1** and **α2** isomer ligands[14,53] and to corroborate Tc^V and Re^V substitution into the α$_1$- and α$_2$- frameworks, *vide infra*.) The ^{31}P NMR spectra along with the ^{183}W spectra are presented in **Figure 2 and Figure S4** for **Tc^{V}O-α1** and **Tc^{V}O-α2**. The ^{31}P NMR spectra establish that the purity of the Tc^V complexes of **α1** and **α2** are greater than 98%. Two resonances are observed for the **Tc^{V}O-α1** and **Tc^{V}O-α2** species. The upfield resonance is assigned to P1, the phosphorous atom close to the Tc^V center, and the remote phosphorous, P2, is assigned to the downfield resonance.

^{183}W NMR is used for structural identification of the Tc^V complexes in solution. Each magnetically inequivalent tungsten atom presents one resonance, with P coupling and W-O-W coupling if the concentration, and thus intensity and resolution, is high enough. The **Tc^{V}O-α2** clearly shows 9 well-resolved resonances with appropriate integrations for incorporation of the Tc^{V}O center into the cap region of the **α2** lacunary polyoxometalate (**Figure 2**). This spectrum is different from free **α2**.[45,54] Incorporation of the Tc^{V}O center into **α1** is clearly identified by the ^{183}W NMR spectrum (**Figure 2**) as well. In this case **α1** possesses C$_1$ symmetry and 17 resonances are observed in the ^{183}W NMR spectrum of the Tc^V complex. The pattern observed in **Figure 2** is clearly different from the **Tc^{V}O-α2** species and from **α1** and **α2** [45,46]. Although the resonances have not been assigned to specific tungsten atoms, the upfield resonance is likely attributed to a W atom close to the vacancy, *vide infra.* The cause of the upfield shift is discussed in detail in the EXAFS section of this manuscript.

In summary, the mass spectroscopy confirms the expected formulations, and the multinuclear (^{31}P and ^{183}W) NMR spectroscopy are consistent with the Tc^{V}O centers incorporating into the cap and belt

regions of **α2** and **α1** ligands respectively. The isolated, pure species were carried forward for comparison in electrochemical and X-ray Absorption Spectroscopy experiments, *vide infra*.

X-ray absorption fine structure. The x-ray absorption near edge structure (XANES) spectra of TcO_4^-, $TcO_2 \bullet 2H_2O$, $TcO_2 \bullet xH_2O$, **Tc^VO-α1** and **Tc^VO-α2** are shown in **Figure 3**. In this case, the energy of the absorption edge is a reflection of the amount of screening experienced by the 1s electrons. For this reason, the absorption edges of complexes with higher oxidation states typically occur at higher energies of than those of complexes with lower oxidation states. This trend can, however, be complicated by the effects of covalency, which can shift the energy of the absorption edge from what would be expected on the basis of formal oxidation state alone. In the case of the complexes shown in **Figure 3**, the effects of covalency are anticipated to be minor compared with the effects of oxidation state. The half-height of the edges of $TcO_2 \bullet 2H_2O$, **Tc^VO-α1** and **Tc^VO-α2** with respect to that of TcO_4^- are -6.7 eV, -3.2 eV, and -3.7 eV, respectively. The relative position of the Tc K-edge absorption edges of **Tc^VO-α1** and **Tc^VO-α2** with respect to $TcO_2 \bullet 2H_2O$ are consistent with the presence of Tc(V). In addition, the Tc center in **Tc^VO-α2** is slightly more electron rich than that of **Tc^VO-α1**.

The XANES spectra also contain information about the symmetry of the coordination environment in **Tc^VO-α1** and **Tc^VO-α2**. The small, well-defined peaks below 21050 eV are pre-edge features due to the 1s-4d transition, which is symmetry forbidden in centrosymmetric complexes. The presence of this feature in the spectra of **Tc^VO-α1** and **Tc^VO-α2** is consistent with the postulated, non-centrosymmetric structure.

Extended x-ray absorption fine structure (EXAFS) spectra can be used to determine the local structure of a particular chemical element. The Tc K-edge solution EXAFS of **Tc^VO-α1** and **Tc^VO-α2** are shown **Figure 4** along with the EXAFS spectra of model complexes derived by fitting the data. To determine the local structure of the Tc sites, model complexes were created by replacing a tungsten atom in the cap (**Tc^VO-α2**) or the belt (**Tc^VO-α1**) of the Wells-Dawson plenary ion by a Tc center. The

data was fit using shells of scattering atoms at increasing distances from the Tc center. If the value of reduced chi-squared decreased, the scattering shells were retained. The numbers of heavy atom (W, P) neighbors and nearest O neighbors were determined from the model, but the number of more distant oxygen neighbors were determined by varying this number to obtain the best fit.

Tc^VO-α2: The local structure obtained by fitting EXAFS spectrum of **Tc^VO-α2** complexes is consistent with the structure of the cap W site of the Wells-Dawson ion. The distances from the Tc atom to the neighboring atoms are given in **Table 3**.[55] In this case, p(F) for all scattering atoms are less then 0.05, so all atoms can be considered to be observed in the EXAFS experiment. The structure is consistent with a square pyramidal Tc(V). The oxygen coordination environment contains a very short Tc-O bond, 1.64 Å, which is consistent with the terminal oxo ligand of a Tc(V) ion, and the best fit is obtained with 4 oxygen ligands at 2.00 Å and a more distant oxygen neighbor at 2.53 Å. Scattering from more distance atoms, particularly P and W are consistent with coordination of the Tc(V) ion by $(\alpha_2\text{-}P_2W_{17}O_{61})^{10-}$. The best fit is obtained with 2 neighboring W atoms at 3.43 Å, 1 neighboring P atom at 3.54 Å, and 2 more neighboring W atoms at 3.57 Å, in good agreement with the distances predicted if a W atom in the cap of the Wells-Dawson ion is replaced by a Tc atom. The major difference is that terminal oxo of Tc(V) is much shorter than the terminal oxo of W(VI).

EXAFS data collected at the Advanced Photon Source, Argonne National Laboratory, (**Figure S5**, **Table S2**) on the **Tc^VO-α2** are in excellent agreement with the above results. The Tc atom is 6-coordinate with oxygen atoms at: 1.63(1) Å (Tc^VO), 1.93(2) Å and 2.36(2) Å. The results from the APS futher show W atoms at 3.43(3) Å and 3.57 (3) Å, a P atom at 3.48(3) Å and an O atom at 3.98(4) Å, which is consistent with Tc(V) coordinated to $(\alpha_2\text{-}P_2W_{17}O_{61})^{10-}$.

Tc^VO-α1: Surprisingly, the local structure obtained by fitting the EXAFS spectrum of **Tc^VO-α1** is not consistent with simply replacing a W atom in the belt of the Wells-Dawson ion by a Tc atom as shown by the comparison of the bond distances derived by fitting the EXAFS spectrum with the local structure

of the belt W atoms of the Wells-Dawson ion given in **Table 4**. Initial refinements using this model suggested that Tc possessed a neighboring atom at ~3 Å. Furthermore, fitting of the nearest oxygen shells with a square pyramidal model did not fit the data accurately; an acceptable fit could only be obtained with the typical short Tc(V) bond plus 5 next-nearest oxygen neighbors. The oxygen neighbors suggested that the Tc was in a pseudooctahedral, rather than square pyramidal geometry. Therefore, the initial Tc model was replaced by one with the TcO unit translated by 0.3 Å towards the phosphate oxygen in the center of the Wells-Dawson ion.

The revised model is in good agreement with the EXAFS data. **Tc^{V}O-α1** still possesses the short Tc-O bond, 1.64 Å, typical of Tc(V) but has 5 next-nearest oxygen neighbors at 1.97 Å, rather than the 4 next-nearest oxygen neighbors found in **Tc^{V}O-α2**. The distance to the nearest W atom is only 3.09 Å, which is much shorter than the nearest distance between neighboring W atoms in the belt of the Wells-Dawson ion, 3.37 Å. Likewise, the distance to the phosphorous at next nearest W atoms are shorter than expected. Overall, the data suggest that the Tc(V) center in **Tc^{V}O-α1** has been "pulled into" the Wells-Dawson ion relative to the position of the belt W atom.

A potential explanation for this unexpected structure is suggested by the peak at 37.21 ppm in the ^{183}W NMR spectrum of **Tc^{V}O-α1**. A strong positive shift in the ^{183}W NMR resonances is associated with two scenarios: 2- electron reduced diamagnetic polyoxometalates where the electrons are "delocalized" on the NMR or EPR timescales; this has been reported for the 2e-reduced α-[P$_2$W$_{18}$O$_{62}$]$^{6-}$, [W$_{10}$O$_{32}$]$^{6-}$ and [γ-SiW$_{12}$O$_{40}$]$^{6-}$ species. [56-59] Strong positive shifts are also characteristic of the presence of a metal-metal bonding association. The latter was found for the case of [γ-SiW$_{12}$S$_2$O$_{38}$]$^{6-}$ where the deshielded peaks at +1041 ppm correspond to W^{V} atoms of the {W$_2$O$_2$S$_2$} fragment.[60] The distances between these W^{V} atoms are quite short (2.815 (1) Å), characteristic of a metal-metal bond involving both the W^{V} centers.

In the **Tc^{V}O-α1** case, a similar metal-metal bonding may be occurring: the bonding association

would involve a dative bond from the occupied Tc d_{xy} orbital into the unoccupied d_{xy} orbital of the W atom at 3.09 Å with which the Tc shares an edge. The presence of the Tc-W interaction also explains why the Tc in **Tc^{V}O-α1** is less electron rich than the Tc in **Tc^{V}O-α2** as suggested by the XANES spectrum. The presence of a similar peak in the [183]W NMR spectrum of **Re^{V}O-α1** suggests that this complex possesses a similar metal-metal interaction.

Complexes of **Tc^{V}O-α1** and **Tc^{V}O-α2** that were produced using too little ethylene glycol ("non-optimized" syntheses) were also analyzed by XANES (**Figure S6**) and EXAFS (**Figure S7**, **Tables S3**, **S4** and **S5**). EXAFS analysis taken on **Tc^{V}O-α1** and **Tc^{V}O-α2**, produced by "non-optimized" syntheses, showed the presence of an additional Tc atom at 2.53 – 2.57 Å. The model used to fit the data included either a terminal oxo ligand at 1.75 Å for the Tc(V) species or a Tc atom at 2.53 -2.57 Å for the Tc(IV) species. The origin of this Tc(IV) contribution is likely hydrolysis of the Tc^{V}OCl$_4^-$ starting reagent. The Tc at 2.53-2.57 Å could be due to either reduction of the Tc(V) complex to Tc(IV) followed by dimerization to the Tc^{IV}-(μ-O)$_2$-Tc^{IV} **α1/α2** dimer, or to a Tc^{IV}-(μ-O)$_2$-Tc^{IV} ethyleneglycol complex. Alternatively, the Tc(IV) could be due to a colloidal TcO$_2$•xH$_2$O impurity. However, the results given in **Table S3** and **Table S4** (corresponding to data in **Figures 7a**, and **7b** (data collected two months later) strongly suggest that Tc(IV) is not present as TcO$_2$•xH$_2$O. **Figures S7a** and **S7b** of **Tc^{V}O-α1** show almost identical spectra, and **Tables S3** and **S4** reveal almost identical fit parameters, which suggest that the Tc(IV) present in the sample is resistant to oxidation by atmospheric oxygen. This behavior is not consistent with TcO$_2$•xH$_2$O, which is readily oxidized by oxygen.[61-67] The amount of Tc(IV) in the **Tc^{V}O-α1** sample is significantly greater than in the **Tc^{V}O-α2** sample, but in both cases, the major portion of the technetium is present as a Tc(V) complex as suggested by the XANES data (**Figure S6**).

Electrochemistry. As reported by Nadjo and co-workers,[14] cyclic voltametry (C.V.) is a sensitive technique to identify the **α1** and **α2** isomers, their complexes with transition metals and assess their

purity.   In this study, C.V. has been conducted in aqueous 0.1 M $NaCOOCH_3$ solutions containing 0.5 M $NaSO_4$ at pH 5. The stability of both transition metal-substituted **α1/α2** complexes and **α1/α2** ligands with this combination of supporting electrolyte and pH has been previously demonstrated.[12,14,54]

Figures 5 and **6** compare the C.V.s of **α2** and **α1** lacunary POMs (solid lines) and their respective Tc^VO complexes (dotted lines). In each case, the scans are restricted to a region where no derivitization of the electrode surface is observed; proceeding to more negative potentials can lead to the adsorption of reduced species to the electrode surface. The C.V.s of Tc^VO-**α2** and Tc^VO-**α1** complexes (**Figures 5** and **6** respectively) show new waves that are not observed in the lacunary parents. These waves can be attributed to Tc^{3+}/Tc^{4+}, Tc^{4+}/Tc^{5+}, Tc^{5+}/Tc^{6+} redox couples within the substituted complex. This is analogous to complexes of the **α2** and **α1** isomer containing Cu^{3+} or Fe^{3+} where the reduction of the copper or iron occurs before the reduction of the tungsten centers.[53,68] The observed rest potentials for the samples, and the observation of sharply resolved signals in the ^{31}P NMR (suggestive of diamagnetic species) allow us to assign the waves c.a. -33 and -175 mV (vs Ag/AgCl) as Tc^{4+}/Tc^{5+} redox couples within the **α1** and **α2** complexes respectively. Comparison with the Fe^{2+}/Fe^{3+} wave in the compound **Fe-α1** reveals that this first step consumes one electron per molecule (see **Figure S6**). Waves occurring at more negative potential are attributed to the reduction of the tungsten framework.

The redox waves occurring at more positive potential are assigned as Tc^{5+}/Tc^{6+} redox couples within the substituted complexes (+990 mV for Tc^VO-**α1** and +813 mV for Tc^VO-**α2**). Extending the electrochemical window to more positive potentials allow us to observe a quasi-reversible wave in both compounds. This is assigned to the Tc^{6+}/Tc^{7+} redox process; however, the Tc(VII) species is unstable. Prolonged exposure to positive potentials causes dissociation of the complex into a combination of plenary $(P_2W_{18}O_{62})^{6-}$ and lacunary $(P_2W_{17}O_{61})^{10-}$ Wells-Dawson anions and TcO_4^- (as monitored by ^{31}P and ^{99}Tc NMR). A summary of the observed halfwave potentials is presented in **Table 5**. In

comparison with **Tc^{V}O-α1**, the **Tc^{V}O-α2** complex exhibits an extra wave at a more negative potential (-386 mV), which we are attributing to a Tc^{3+}/Tc^{4+} redox couple.

A comparison of the Tc^{4+}/Tc^{5+} and Tc^{5+}/Tc^{6+} redox couples in the **Tc^{V}O-α1** and **Tc^{V}O-α2** complexes is presented in **Figure 7** and summarized in **Table 6**. The Tc within **Tc^{V}O-α1** is reduced at more positive potentials than the Tc within **Tc^{V}O-α2**. This is consistent with the trend observed for complexes incorporating first row transition metals.[10,12,14,19] The Tc center located in the belt region of the POM (**α1**) undergoes more facile reduction than when located in the cap region (**α2**). This is observed as a difference of 177 mV for the Tc^{5+}/Tc^{6+} redox process and 142 mV for the Tc^{4+}/Tc^{5+} redox process. The more facile reduction of **Tc^{V}O-α1** relative to **Tc^{V}O-α2** may be due the to the Tc-W interaction in **Tc^{V}O-α1**, which should stabilize the lower Tc oxidation states. This highlights the inequivalency of the two sites, and their impact on the chemical properties of transition metal cations substituted in these positions; in this case specifically, the electron transfer properties are unmistakably different.

Figure 8 presents a comparison of the C.V. traces of the Re-substituted **α1** and **α2** complexes, and a summary of the half wave potentials is presented in **Table 5**. A direct assessment of the Re analogues under the same conditions to that of the Tc analyses allow us to correlate the relationships between the substitution position and redox behavior of the metal centers. As with the Tc analogues, new waves at more positive potentials to that of the redox waves of the tungsten framework of the lacunary **α1**and **α2** are observed. Based upon the observed rest potentials and observation of sharp, resolute lines in the ^{31}P NMR spectra (indicative of diamagnetic species), we can assign the waves centered at -445 and -443 mV as Re^{3+}/Re^{4+} redox couples, those at -295 and -284 mV as Re^{4+}/Re^{5+} redox couples, the waves at +477 and +254 mV as Re^{5+}/Re^{6+} redox processes, and the waves at +822 and +627 mV as Re^{6+}/Re^{7+} redox couples (for **Re^{V}O-α1** and **Re^{V}O-α2** respectively). The assignment of

the quasi-reversible waves at +822 and +627 mV as Re^{6+}/Re^{7+} is analogous to those in the Tc complexes.

Once again, prolonged exposure to oxidative potentials (greater that +870 mV) causes the complexes to dissociate irreversibly into a combination of plenary $(P_2W_{18}O_{62})^{6-}$ and lacunary $(P_2W_{17}O_{61})^{10-}$ Wells-Dawson anions and ReO_4^- (as judged by ^{31}P NMR and electrochemistry). A comparison of the various waves is presented in **Table 6**. The redox processes in the belt region consistently occur at potentials of about 200 mV more positive than those of the cap region. This is parallel to what is observed in the Tc examples, albeit the reduction/oxidation of the Re is decidedly more impacted by the substitution i.e, The average $E_{1/2}$(**Re^VO-α1**) – $E_{1/2}$ (**Re^VO-α2**) = 202 mV and the average $E_{1/2}$(**Tc^VO-α1**) – $E_{1/2}$ (**Tc^VO-α2**) = 160 mV.

Upon comparison of the redox couples for **Re^VO-α1 and Re^VO-α2** (**Table 6**), a difference of 223.5 and 181.5 mV is observed for the Re^{5+}/Re^{6+} and the Re^{6+}/Re^{7+} waves, respectively. As with the Tc complexes, this trend is consistent with stabilization of lower oxidation states in **Re^VO-α1** by formation of a Re-W bond. This trend is not apparent for what are assigned as Re^{3+}/Re^{4+} and Re^{4+}/Re^{5+} couples. The difference in the position of the redox waves differ by c.a. -11 mV (vs Ag/AgCl) which indicates that either (i) these waves are actually due to redox processes involving the tungsten framework and the Re^{3+}/Re^{4+} and Re^{4+}/Re^{5+} couples are eclipsed, or (ii) the Re^{3+}/Re^{4+} and Re^{4+}/Re^{5+} couples are unaffected by substitution position. This is currently undergoing investigation using *in-situ* spectroelectrochemistry.

Figure 9 presents a comparison of the C.V.s of the family of **α2** and **α1** complexes. **Figure 9A** shows the voltammograms of **Tc^VO-α2** (dotted line) and **Re^VO-α2** (solid line), **Figure 9B** shows the voltammograms of **Tc^VO-α1** (dotted line) and **Re^VO-α1** (solid line). It can be seen that the reduction of Tc(VI) to Tc(V) is more facile than that of the Re(VI) to Re(V) by 559 mV (**Table 6)** within the cap-substituted **α2** complexes. This trend is paralleled in the **α1** complexes, but the difference between the

M(VI) to M(V) reduction is 512 mV. When comparing the differences in potential for the reduction of M(V) to M(IV), the more favorable process again lies with the Tc complexes, but the ease with which this occurs compared to the Re congener is different between the **α2** (109 mV) and the **α1** (262 mV) complexes.

All the electrochemical studies, described above, along with multinuclear NMR and mass spectrometry clearly confirm that the technetium center present within the structure of the compounds **Tc^{V}O-α1** and **Tc^{V}O-α2** is in the +V oxidation state. This Tc(V) center can be reduced to Tc(IV) or oxidized to Tc(VI). Other oxidation states (+III and +VII) have been identified in other electrolytes and these studies will be published elsewhere.

CONCLUSION

Understanding and controlling the extensive redox chemistry of ^{99}Tc is one of the obstacles in identifying separation strategies, and the identification and development of appropriate waste-forms for containing ^{99}Tc once separated from nuclear fuel and waste tanks. We are approaching this problem from a molecular-level vantage point by employing polyoxometalates to address the coordination chemistry and redox stability of Tc within metal oxide matrices.

In this study we report the synthesis and physical chemical properties of Tc^{V}O incorporated into the lacunary **α1** and **α2** polyoxometalates. These syntheses rely on the use of a "transfer ligand", ethylene glycol, which facilitates the stabilization of the Tc^{V}O core as the complexes are formed. The complexes were characterized by multinuclear NMR spectroscopy, X-ray spectroscopy and electrochemistry. Together, these techniques provide compelling evidence that the Tc(V) is incorporated in the **α1** and **α2** frameworks.

Transition metal cations substituted into the **α1** and **α2** positions clearly show differences in electrochemistry; specifically, transition metal cations substituted into the **α1** position are more readily

reduced than when substituted in the **α2** position.[10,12,14,19] These differences may be explained by the differences in the local structures of Tc in these complexes as determined by EXAFS. The ease of reduction for metal ions coordinated in the α_1 position is consistent with the formation of dative metal-metal bond between Tc(V) and the nearest tungsten atom in the lacunary Wells-Dawson ion. The defects of **α1** and **α2** are shown in **Figure 10**. The basic oxygen of the **α1** defect (gray in **Figure 10**) is bound to the phosphorous atom and one tungsten atom; in contrast the corresponding oxygen of the **α2** defect is bound to the one phosphorous atom and two tungsten atoms. The oxygen of the **α1** site would thus favor stronger interaction of the transition metal with the W atoms in the belt. Theoretical treatments are consistent with these findings; the LUMO in the frontier orbitals of the parent (α-$P_2W_{18}O_{61}$)$^{6-}$ (a''$_1$) consists of 96% α1 character.[69]

This reduction behavior is illustrated in this study wherein Tc^{V}O is substituted into the **α1** and **α2** defects. The reduction of Tc(V) to Tc(IV) indeed is facilitated in the **Tc^{V}O-α1** isomer compared to the **Tc^{V}O-α2** isomer (+157 mV). To evaluate and quantify the influence due to the specific isomers, we must operate under conditions where the influence of protonation is negligible, i.e. at pH equal or greater than 7. A full electrochemical study as a function of pH and comparison with DFT calculations to compare the energies of **Tc^{V}O-α1** and **Tc^{V}O-α2** will be forthcoming.

ACKNOWLEDGMENT

SUPPORTING INFORMATION PARAGRAPH Supporting Information consists of Figures showing the column purification of **Re^{V}O-α1** (**Figure S1**); Infrared Spectra of **Tc^{V}O-α1** and **Tc^{V}O-α2** (**Figure S2**); Mass Spectra for **Tc^{V}O-α1** and **Tc^{V}O-α2** (**Figure S3**); ^{183}W NMR for an independent synthesis of **Tc^{V}O-α1** (**Figure S4**); EXAFS data for **Tc^{V}O-α2** taken at the Advanced Photon Source, Argonne National Laboratory (**Figure S5**). XANES and EXAFS data for non-optimized syntheses of **Tc^{V}O-α1** where the Tc^{IV}-(μ-O)$_2$-Tc^{IV} species was identified are shown in **Figure S6**, XANES and **Figures S7a** , **S7b** and **S7c**, EXAFS); Also included are the CVs of **Tc^{V}O-α1** and **Fe-α1** (**Figure S8**). Supporting Material Tables include: **Table S1** showing ^{31}P NMR data monitoring the progress of the reaction progress of **Tc^{V}O-α2**; **Table S2** showing best fit parameters for **Tc^{V}O-α2** taken at the APS at Argonne, **Tables S3**, **S4** showing the best fit parameters for the EXAFS spectra for non-optimized syntheses of **Tc^{V}O-α1** where the Tc^{IV}-(μ-O)$_2$-Tc^{IV} species was identified (shown in **Figure S7a** and **S7b**); **Table S5** showing best fit parameters for non-optimized syntheses of **Tc^{V}O-α2** where the Tc^{IV}-(μ-O)$_2$-Tc^{IV} species was identified (**Figure S7c).**

FIGURE CAPTIONS.

Figure 1. The plenary Wells-Dawson ion and lacunary Wells-Dawson isomers. Top: polyhedral representation; Bottom: ball and stick representation. A: $(\alpha\text{-}P_2W_{18}O_{62})^{6-}$ is the "plenary" or parent Wells-Dawson ion, ca. 1.2 nm in length and 0.6 nm width; B: removal of a "belt" W from the plenary Wells-Dawson structure gives the "lacunary" $(\alpha_1\text{-}P_2W_{17}O_{61})^{10-}$ isomer; C: removal of a "cap" W from the plenary Wells-Dawson gives the $(\alpha_2\text{-}P_2W_{17}O_{61})^{10-}$ isomer. The terminal oxygen atoms in the defects are shown in cyan. The defect structures possess distinct and different electronic and steric features that impact chemical and redox speciation of ^{99}Tc.

Figure 2: Multinuclear NMR Data for **Tc^{V}O-α1** and **Tc^{V}O-α2** taken at 25°C in D$_2$O. Top: ^{31}P NMR data; bottom: ^{183}W NMR data.

Figure 3. Tc K-edge XANES spectra of, from lowest energy to highest energy, TcO$_2$•2H$_2$O (black), **Tc^{V}O-α2** (green), **Tc^{V}O-α1** (orange), and TcO$_4^-$ (blue). Data obtained using SSRL beam line 4-1.

Figure 4. Tc K-edge EXAFS spectra (left) and Fourier transforms (right) for **Tc^{V}O-α1** (upper) **Tc^{V}O-α2** (lower). Data are shown in color and fits are given in black. Data obtained using SSRL beam line 4-1.

Figure 5. Cyclic Voltammograms of **α2** (solid line) and **Tc^{V}O-α2** (dashed line) in 0.1 M CH$_3$COONa/CH$_3$COOH containing 0.5 M NaSO$_4$, pH = 5.00. Working electrode: glassy carbon, auxiliary electrode: platinum wire, reference electrode: Ag/AgCl. Scan rate = 10 mVs^{-1}.

Figure 6. Cyclic Voltammograms of **α1** (solid line) and **Tc^{V}O-α1** (dashed line) in 0.1 M CH$_3$COONa/CH$_3$COOH containing 0.5 M NaSO$_4$, pH = 5.00. Working electrode: glassy carbon, auxiliary electrode: platinum wire, reference electrode: Ag/AgCl. Scan rate = 10 mVs^{-1}.

Figure 7. Cyclic Voltammograms of **Tc^{V}O-α1** (solid line) and **Tc^{V}O-α2** (dashed line) in 0.1 M CH$_3$COONa/CH$_3$COOH, containing 0.5 M NaSO$_4$, pH = 5.00. Working electrode: glassy carbon; auxiliary electrode: platinum wire; reference electrode: Ag/AgCl. Scan rate 10 mVs^{-1}.

Figure 8. Cyclic Voltammograms of **Re^{V}O-α1** (solid line) and **Re^{V}O-α2** (dotted line) in 0.1 M CH$_3$COONa/CH$_3$COOH containing 0.5 M NaSO$_4$, pH = 5.00. Working electrode: glassy carbon, auxiliary electrode: platinum wire, reference electrode: Ag/AgCl. Scan rate = 10 mVs^{-1}.

Figure 9. Cyclic Votammograms of Tc and Re complexes; A: **Re^{V}O-α2** (solid line) and **Tc^{V}O-α2** (dotted line). B: **Re^{V}O-α1** (solid line) and **Tc^{V}O-α1** (dotted line) in 0.1 M CH$_3$COONa/CH$_3$COOH containing 0.5 M NaSO$_4$, pH = 5.00. Working electrode: glassy carbon, auxiliary electrode: platinum wire, reference electrode: Ag/AgCl. Scan rate = 10 mVs^{-1}.

Figure 10. Representations of the defect sites of **α2** and **α1**. The tungsten atoms that create the defect are shown as balls. The tungsten atoms not closely associated with the defect site are represented as octahedra. The oxygen atoms bound to the W atoms of the defect are shown in green. All other oxygen atoms bound to W atoms are shown in red. The P atoms are yellow. The oxygen atom bound to the phosphorous of the defect is shown in off white. In the **α2** site, this oxygen atom is bound to two W atoms and the P atom; in the **α1** site, this oxygen atom is bound to one W atom and the P atom.

TABLES

Table 1. Multinuclear NMR Data for Tc^V- α_1/α_2-$P_2W_{17}O_{61}$ complexes.[a]			
Compound	Solvent[b]	^{31}P NMR, δ (ppm)[c]	^{183}W NMR, δ (ppm)
Tc^VO-$\alpha2$	D_2O	-11.60 (1), -13.16 (1)	-131.059 (2), -161.506 (1), -179.912 (2), -181.720 (2), -192.189 (2), -195.228 (2), -199.685 (2), -214.819 (2), -228.776 (2)
Tc^VO-$\alpha1$	D_2O	-11.60 (1), -12.72 (1)	37.21 (1), -117.85 (1), -120.78 (1), -132.83 (1), -147.71 (1), -172.40 (1), -173.08 (1), -174.01 (1), -185.67 (1), -188.84 (1), -189.09 (1), -190.01 (2), -203.29 (1), -204.70 (2), -229.39 (1)
Re^VO-$\alpha1$	D_2O	-12.02 (1), -12.33 (1)	35.17(1), -108.55(1), -111.43(1), -157.35(1), -167.90(1), -180.02(2), -184.51(1), -197.41(1), -208.1 (2), -228.77(1), -237.95(1), -242.69(1), -258.18(1), -308.79(1), -398.52(1).
a. See text for conditions. All spectra were taken at room temperature, 25°C.			

Table 2. Mass Spectrometry of the Tc^V- α_1/α_2-$P_2W_{17}O_{61}$ complexes		
Compound	**Ion**	**m/z**
Tc^VO-$\alpha2$		
	$K_4HTcO[P_2W_{17}O_{61}]^{2-}$	2217.9
	$K_4TcO[P_2W_{17}O_{61}]^{3-}$	1478.5
	$K_3HTcO[P_2W_{17}O_{61}]^{3-}$	1465
	$K_2H_2TcO[P_2W_{17}O_{61}]^{3-}$	1453
	$KH_3TcO[P_2W_{17}O_{61}]^{3-}$	1440
	$H_4TcO[P_2W_{17}O_{61}]^{3-}$	1427
	$K_2HTcO[P_2W_{17}O_{61}]^{4-}$	1089.6
	$KH_2TcO[P_2W_{17}O_{61}]^{4-}$	1080.2
	$H_3TcO[P_2W_{17}O_{61}]^{4-}$	1070.7
Tc^VO-$\alpha1$	$K_4HTcO[P_2W_{17}O_{61}]^{2-}$	2217.8
	$K_4TcO[P_2W_{17}O_{61}]^{3-}$	1477.6
	$K_3HTcO[P_2W_{17}O_{61}]^{3-}$	1465
	$K_3TcO[P_2W_{17}O_{61}]^{4-}$	1099
	$K_2HTcO[P_2W_{17}O_{61}]^{4-}$	1089.8
	$KH_2TcO[P_2W_{17}O_{61}]^{4-}$	1079.1
	$H_3TcO[P_2W_{17}O_{61}]^{4-}$	1070.3

Table 3: Best fit parameters for the EXAFS spectrum for K^+ salt of Tc^VO-α2

Neighbor	# of Neighbors[b]	Distance (Å)	σ^2 (Å^2)	p(F)[b]	Local structure of the "cap" tungsten site (Å)[c]
O	1	1.638(4)	0.0014(5)	<0.001	1.72
O	4	1.996(4)	0.0025(2)	<0.001	1.93
O	1	2.53(2)	0.0025(2)[d]	0.016	2.33
W	2	3.43(2)	0.003(1)	0.011	3.38
P	1	3.54(5)	0.003(1)[d]	0.018	3.52
W	2	3.57(2)	0.004(2)	<0.001	3.62
O	6	3.97(2)	0.002(1)	0.002	6 from 3.7 to 4.1
O (MS)	2	4.28(7)	0.002(1)[d]	0.034	4.05
O	6	4.47(1)	0.002(1)[d]	<0.001	8 from 4.3 to 4.6 Å

a) Fit range: $2<k<15$, $1.1<R<3.9$, 30 independent data. 15 parameters, $S_0^2 = 0.9$, $\Delta E_0 = 71()$ eV, $\chi^2 = 25$, $\chi_v^2 = 2$, $R = 0.09$.
b) F-test determines the significance of the improvement to the fit created by adding an additional set of atoms. If the p-value is less than 0.05, the additional atoms have significantly improved the fit and can be considered "observed" in the EXAFS experiment.
c) Dawson, B. Acta. Cryst. 1953, 6, 113 – 126.
d) Debye-Waller of this shell constrained to be equal to that of the preceding shell.
e) Multiple scattering from the mutually *trans* oxygen ligands

Table 4: Best fit parameters for the EXAFS spectrum for Tc^{V}O-α1

Neighbor	# of Neighbors[b]	Distance (Å)	σ^2 (Å^2)	p(F)[b]	Local structure of the "belt" tungsten site[c]
O	1	1.640(3)	0.0013(4)	<0.001	1.72
O	5	1.974(2)	0.0033(2)	<0.001	2.01
W	1	3.087(4)	0.0022(5)	0.014	3.37
P	1	3.394(5)	0.0022(15)[d]	0.042	3.51
O	5	3.31(4)	0.02(1)	0.054	8 from 3.5 to 4.1
W	3	3.456(7)	0.0068(7)	<0.001	3.72
O (multiple scatter)[e]	6	4.08(2)	0.004(3)	0.001	4.05
O	4	4.44(2)	0.005(2)^2	0.032	5 from 4.4 to 4.5 Å

a) Fit range: 2<k<14, 1<R<5; 33 independent data. 16 parameters, $S_0^2 = 0.9$, $\Delta E_0 = 4.2(9)$ eV, $\chi^2 = 428$, $\chi_v^2 = 26$, R = 0.009.
b) F-test determines the significance of the improvement to the fit created by adding an additional set of atoms. If the p-value is less than 0.05, the additional atoms have significantly improved the fit and can be considered "observed" in the EXAFS experiment.
c) Dawson, B. Acta. Cryst. 1953, 6, 113 – 126.
d) Debye-Waller of this shell constrained to be equal to that of the preceding single-scattering shell.
e) Multiple scattering due to mutually *trans* oxygen ligands

Table 5. Halfwave potentials for the electroactive Tc^{V}O and Re^{V}O substituted within the α1 and α2 frameworks at pH 5; scan rate 10 mVs^{-1}.

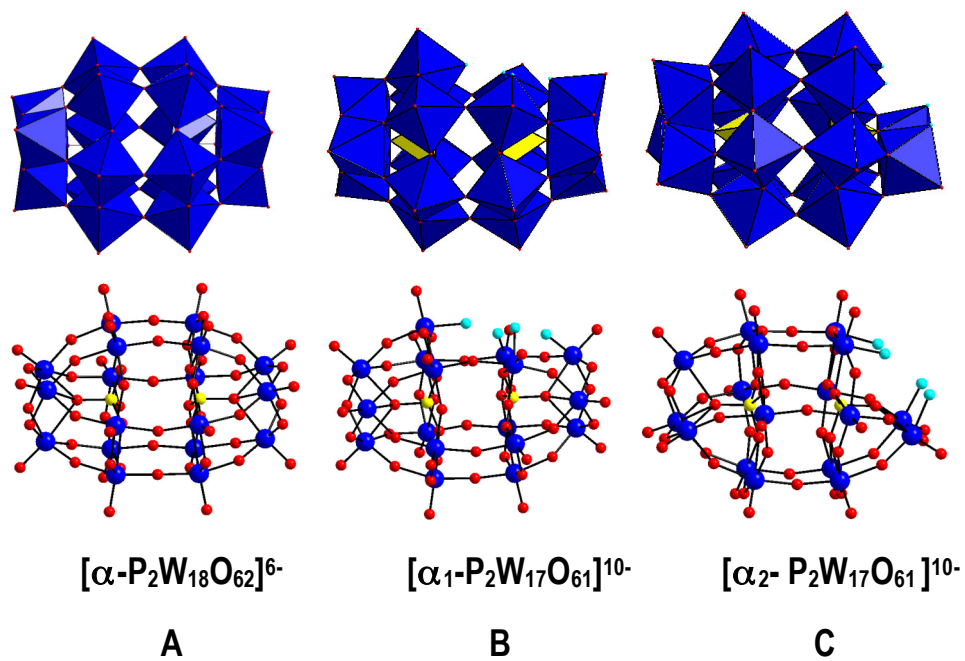| Compound	M$^{6+/7+}$ (mV)	M$^{5+/6+}$ (mV)	M$^{4+/5+}$ (mV)
Tc^{V}O-α1	n/a	990	-33
Tc^{V}O-α2	n/a	813	-175
Re^{V}O-α1	811.5	477.5	-295
Re^{V}O-α2	630	254	-284

Table 6. Summary of the differences in the half-wave potentials between **Tc^{V}O-α1**/**Tc^{V}O-α2** and **Re^{V}O-α1**/**Re^{V}O-α2** complexes and the differences between the Tc and Re complexes.
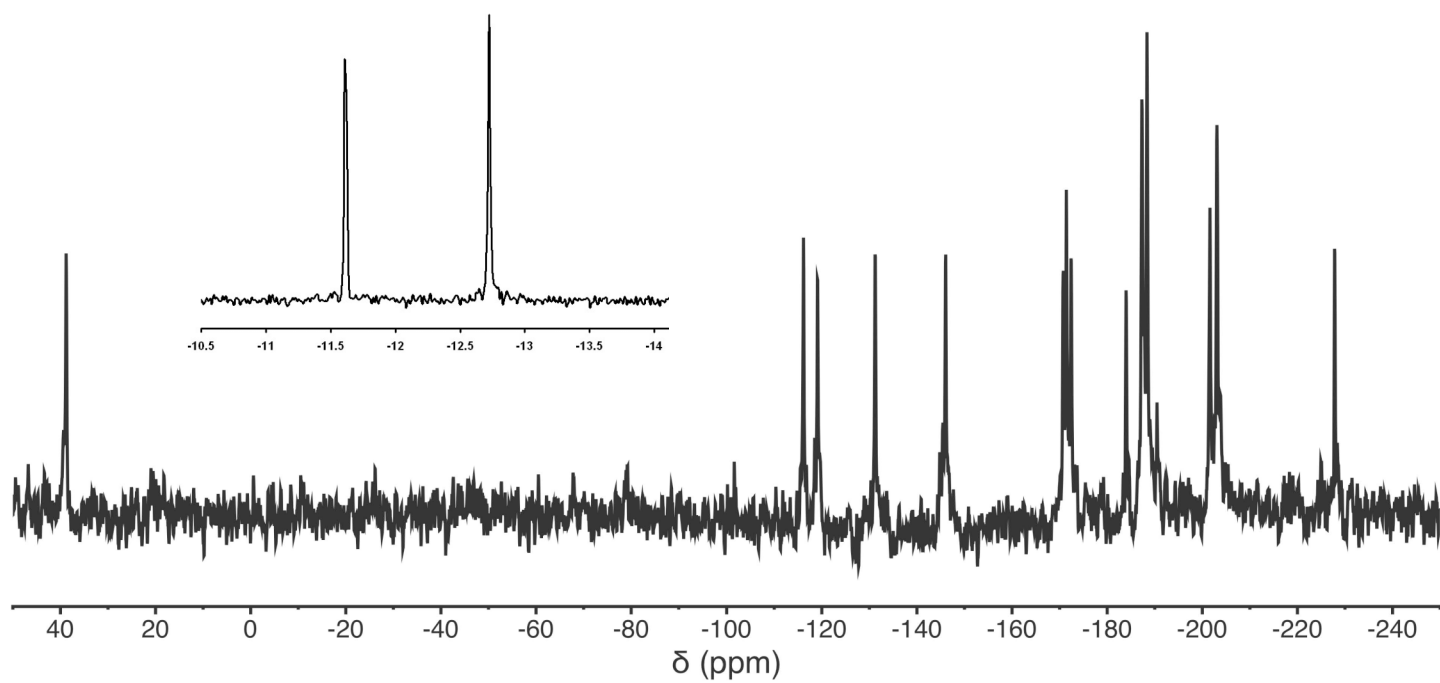
Compound	M$^{6+/7+}$ (mV)	M$^{5+/6+}$ (mV)	M$^{4+/5+}$ (mV)
Tc^{V}O-α1 - **Tc^{V}O-α2**	n/a	177	142
Re^{V}O-α1 - **Re^{V}O-α2**	181.5	223.5	-11
Tc^{V}O-α1 - **Re^{V}O-α1**	n/a	512.5	262
Tc^{V}O-α2 - **Re^{V}O-α2**	n/a	559	109

FIGURES

Figure 1

$[\alpha\text{-}P_2W_{18}O_{62}]^{6-}$

$[\alpha_1\text{-}P_2W_{17}O_{61}]^{10-}$

$[\alpha_2\text{-}P_2W_{17}O_{61}]^{10-}$

A

B

C

Figure 2

TcO α_1- $P_2W_{17}O_{61}$ $^{7-}$
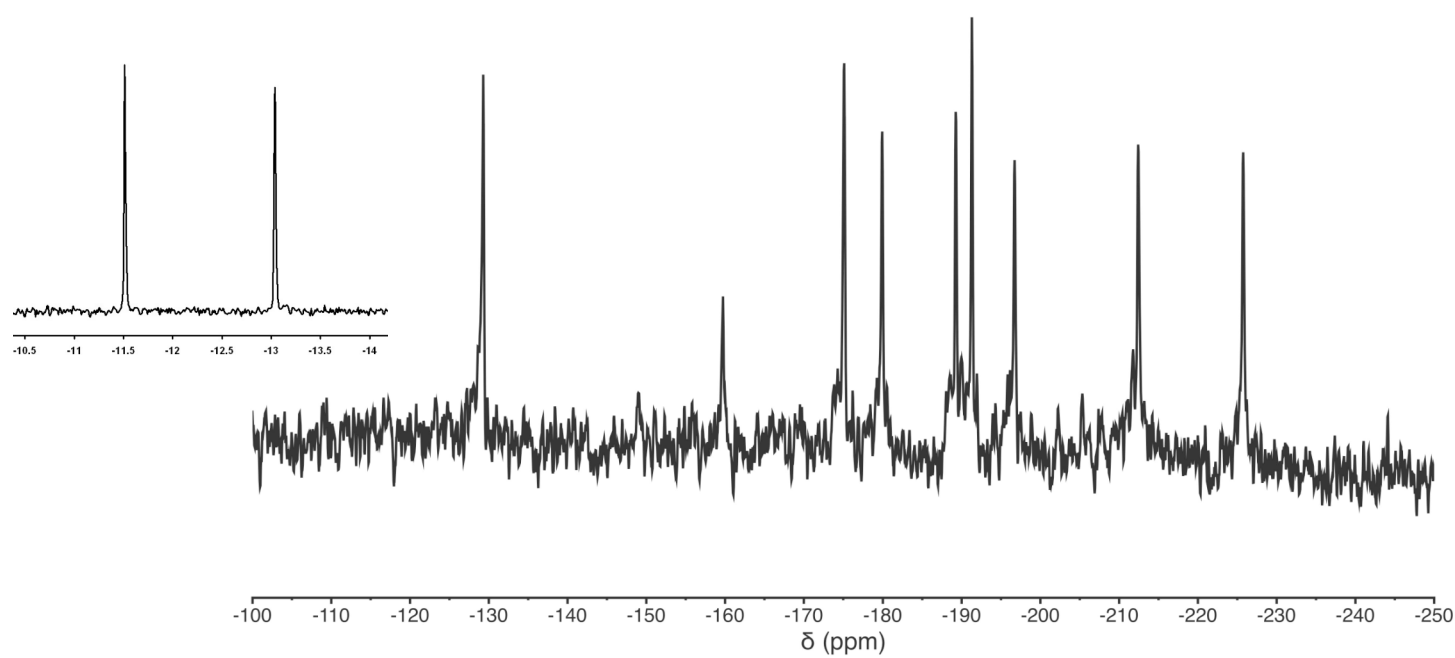
TcO α_2- $P_2W_{17}O_{61}$ $^{7-}$
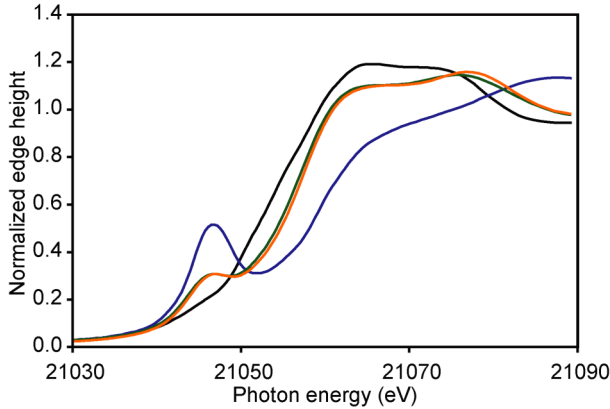
Figure 3

Figure 4
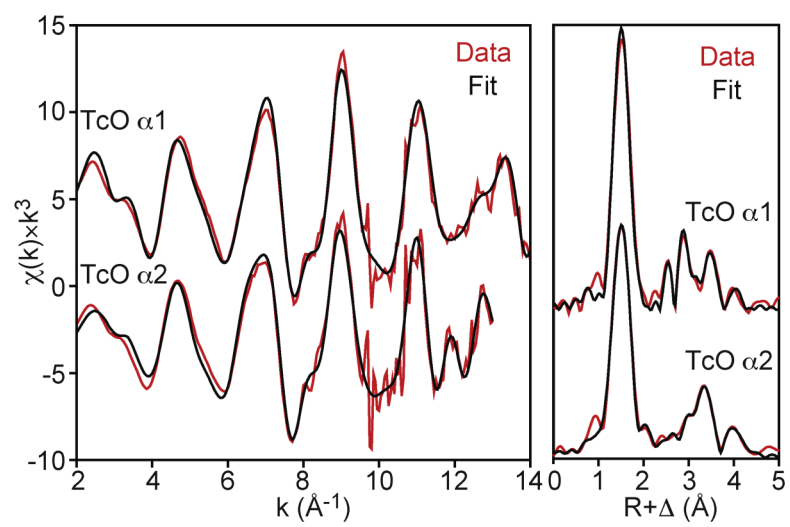
Figure 5

Figure 6

Figure 7

Figure 8

Figure 9
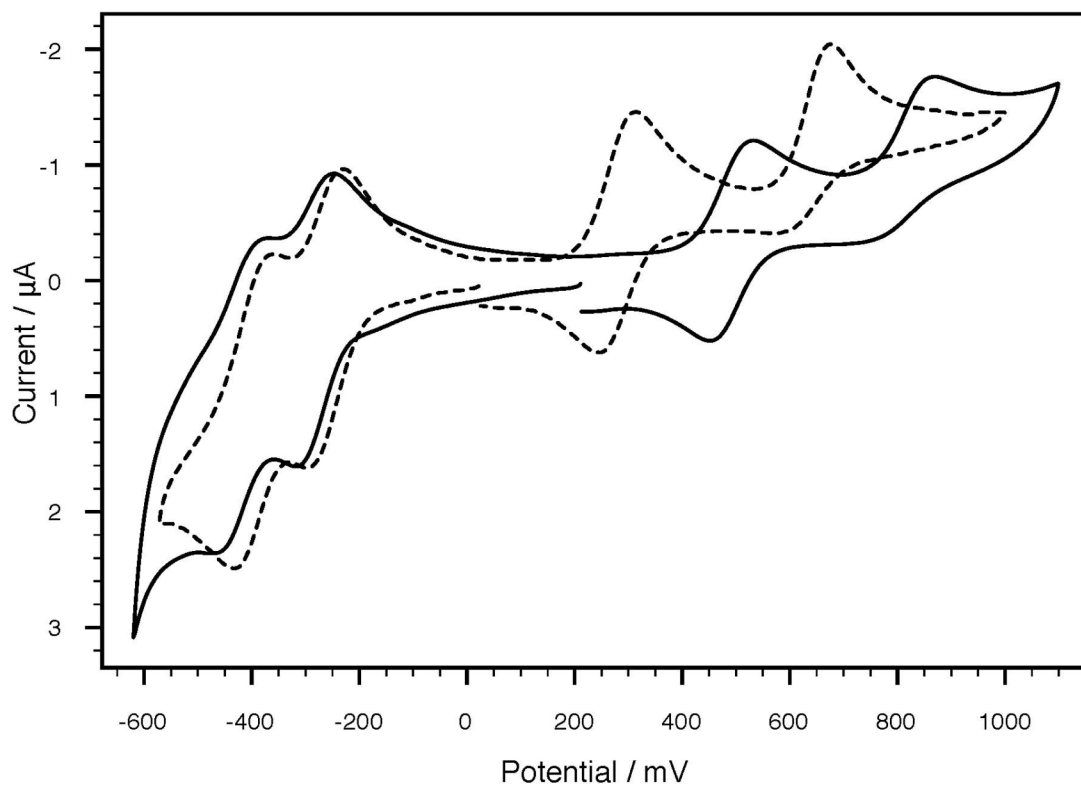
Figure 10
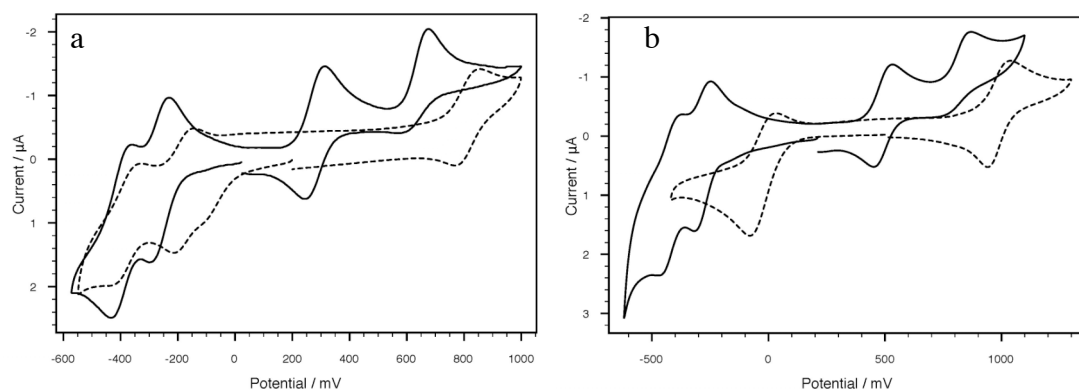
$\alpha_2\text{-} P_2W_{17}O_{61}^{10-}$ $\alpha_1\text{-} P_2W_{17}O_{61}^{10-}$
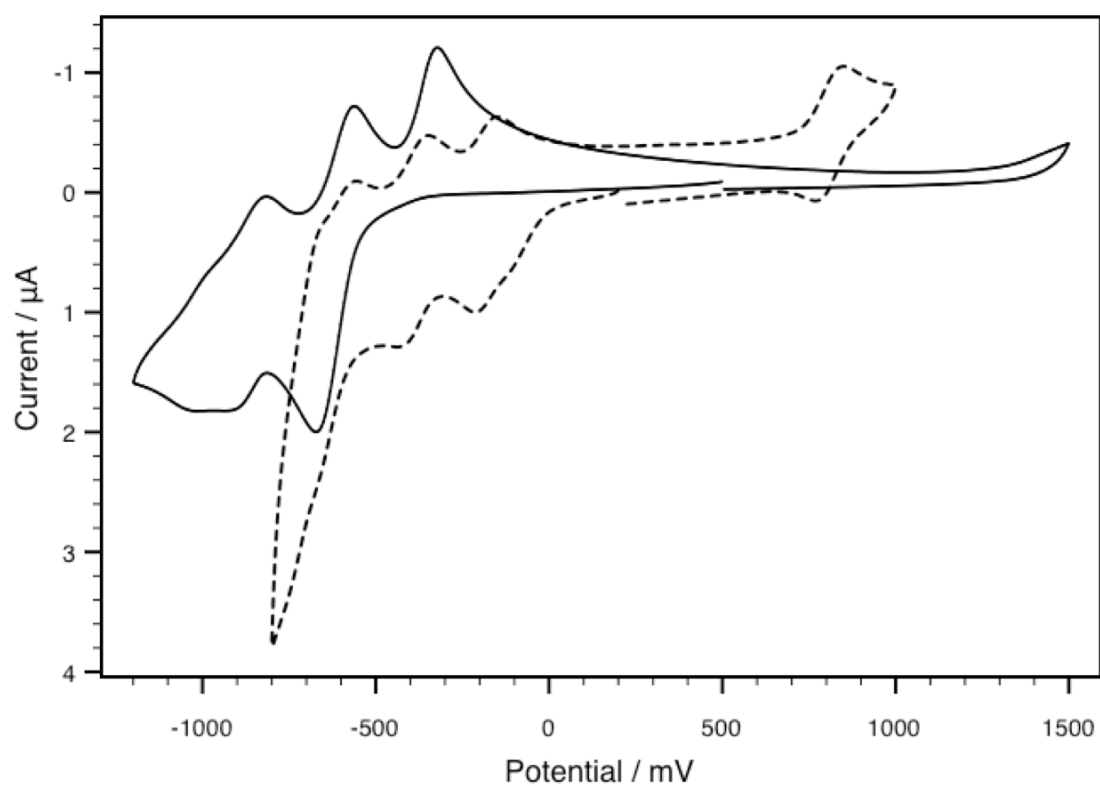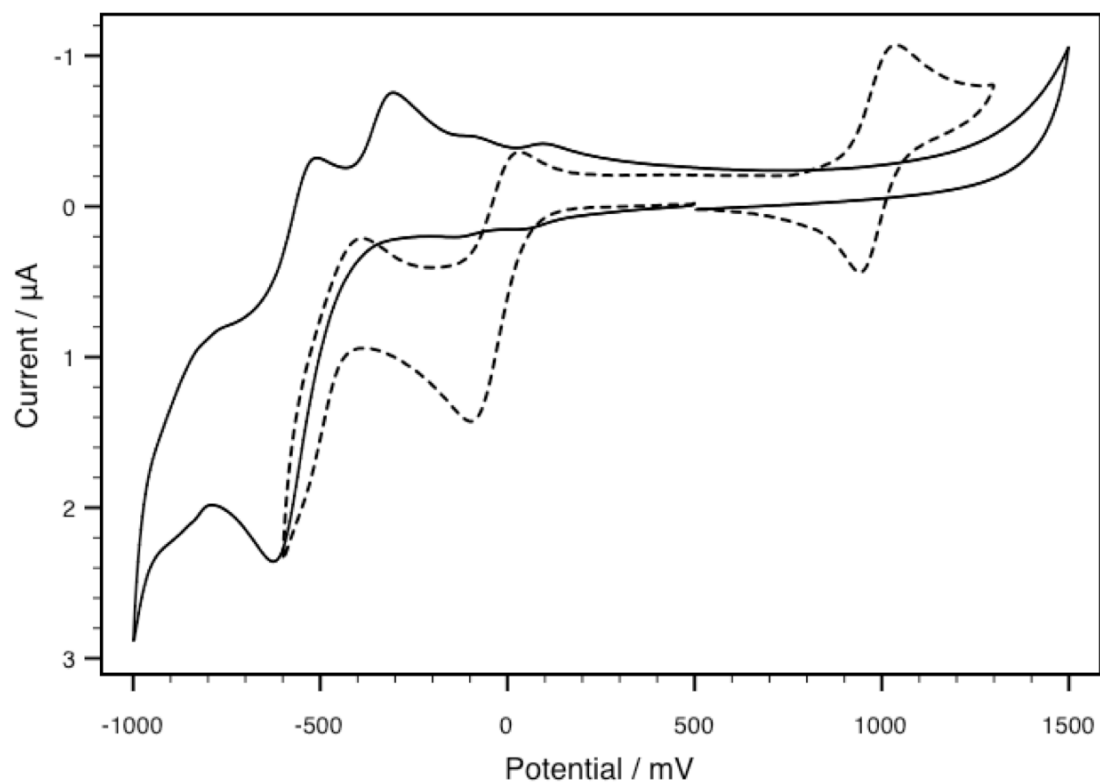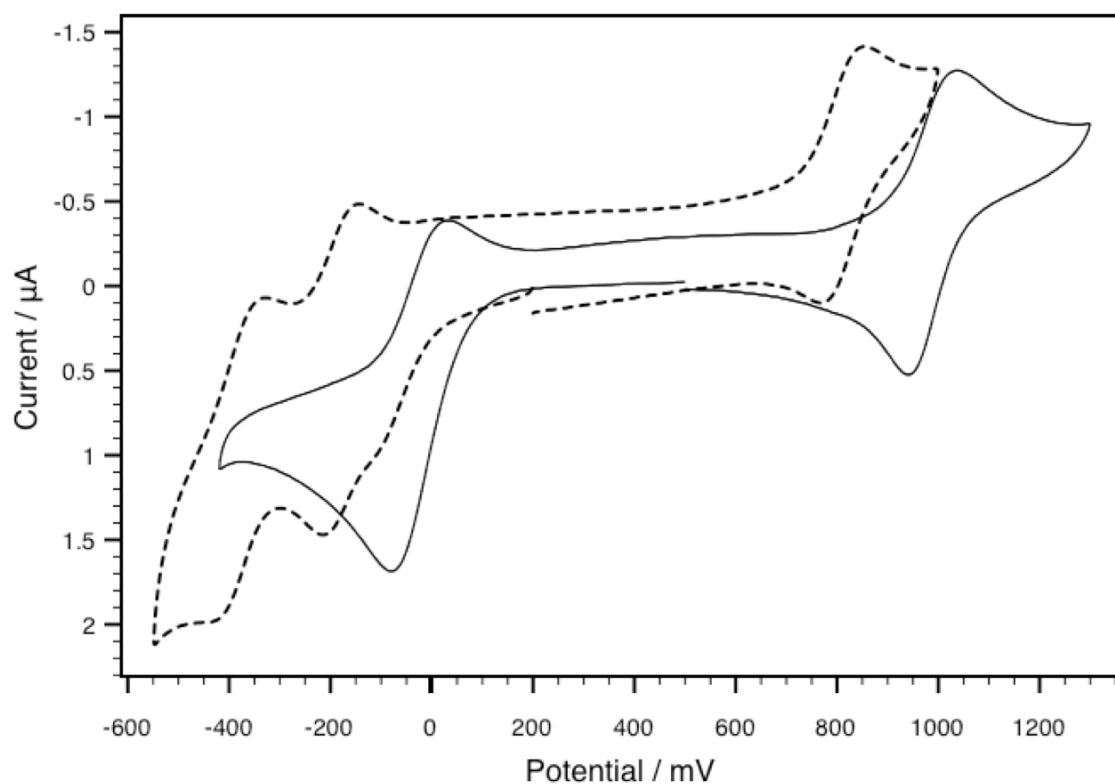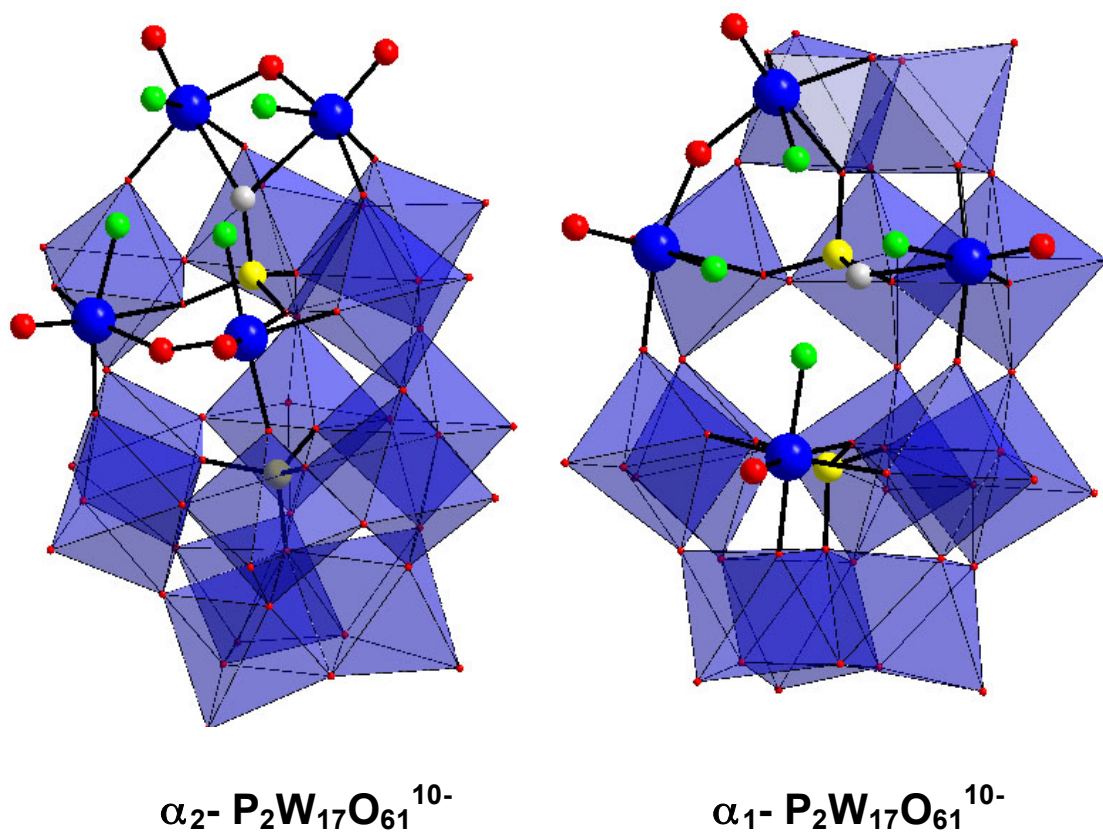
REFERENCES

(1)   Beals, D. M.; Hayes, D. W. *Sci. Total Environ.* **1995**, *173*, 101.

(2)   Hunt, A. G.; Skinner, T. E. *Hydrogeol. J.* **2010**, *18*, 381.

(3)   Fang, X.; Hill, C. L. *Angew. Chem. Int. Ed.* **2007**, *46*, 3877.

(4)   Day, V. W.; Klemperer, W. G.; Schwartz, C.; Wang, R.-C. In *Surface Organometallic Chemistry: Molecular Approaches to Surface Catalysis*; Kluwer Academic Publishers: New York, 1988, p 173.

(5)   Long, D.-L.; Burkholder, E.; Cronin, L. *Chem. Soc. Rev.* **2007**, *36*, 105.

(6)   Day, V. W.; Klemperer, W. G. *Science* **1985**, *228*, 533.

(7)   Abbessi, M.; Contant, R.; Thouvenot, R.; Herve, G. *Inorg. Chem.* **1991**, *30*, 1695.

(8)   Boglio, C.; Lenoble, G.; Duhayon, C.; Hasenknopf, B.; Thouvenot, R.; Zhang, C.; Howell, R. C.; Burton-Pye, B. P.; Francesconi, L. C.; Lacote, E.; Thorimbert, S.; Malacria, M.; Afonso, C.; Tabet, J.-C. *Inorg. Chem.* **2006**, *45*, 1389.

(9)   Ciabrini, J.-P.; Contant, R. *J. Chem. Research (S) 1993, 391* **1993**, 2720.

(10)   Contant, R.; Abbessi, M.; Canny, J.; Belhouari, A.; Keita, B.; Nadjo, L. *Inorg. Chem.* **1997**, *36*, 4961.

(11)   Contant, R.; Ciabrini, J.-P. *J. Chem. Research (S) 1982, 50-51* **1982**, *1982*, 641.

(12)   Contant, R.; Richet, M.; Lu, Y. W.; Keita, B.; Nadjo, L. *Eur. J. Inorg. Chem.* **2002**, 2587.

(13)   Harmalker, S. P.; Leparulo, M. A.; Pope, M. T. *J. Amer. Chem. Soc.* **1983**, *105*, 4286.

(14)   Keita, B.; Girard, F.; Nadjo, L.; Contant, R.; Canny, J.; Richet, M. *Journ. of Electroanal. Chem.* **1999**, *478*, 76.

(15)   Leparulo-Loftus, M. A.; Pope, M. T. *Inorg. Chem.* **1987**, *26*, 2112.

(16)   Sadakane, M.; Dickman, M. H.; Pope, M. T. *Inorg. Chem.* **2001**, *40*, 2715.

(17)   Sadakane, M.; Ostuni, A.; Pope, M. T. *J. Chem. Soc. Dalton Trans.* **2002**, 63.

(18)   Zhang, C.; Howell, R. C.; Luo, Q.; Fieselmann, H. L.; Todaro, L.; Francesconi, L. C. *Inorg. Chem.* **2005**, *44*, 3569.

(19)   Contant, R.; Herve, G. *Reviews in Inorganic Chemistry* **2002**, *22*, 63.

(20)   Contant, R.; Thouvenot, R. *Inorganica Chimica Acta* **1993**, *212*, 41.

(21)   *The inorganic chemistry of technetium and rhenium as relevant to nuclear medicine*; Deutsch, E.; Libson, K.; Vanderheyden, J.-L., Eds.; Cortina International: Verona, 1990; Vol. 3.

(22)   Libson, K.; Woods, M.; Sullivan, J.; Watkins II, J. W.; Elder, R. C.; Deutsch, E. *Inorganic Chemistry* **1988**, *27*, 999.

(23)   VanderHeyden, J.-L.; Heeg, M. J.; Deutsch, E. A. *Inorganic Chemistry* **1985**, *24*, 1666.

(24)   Abrams, M. J.; Costello, C. E.; Shaikh, S. N.; Zubieta, J. *Inorg. Chim. Acta* **1991**, *180*, 9.

(25)   Ortega, F.; Pope, M. T. *Inorg. Chem.* **1984**, *23*, 3292.

(26)   Venturelli, A.; Nilges, M. J.; Smirnov, A.; Belford, R. L.; Francesconi, L. C. *J. Chem. Soc., Dalton Trans.* **1999**, 301.

(27)   Kato, C. N.; Hara, K.; Hatano, A.; Gogo, K.; Kuribayashi, T.; Hayashi, K.; Shinohara, A.; Kataoka, Y.; Mori, W.; Nomiya, K. *Eur. J. Inorg. Chem.* **2008**, *2008*, 3134.

(28)   Boyd, G. E. *J. Chem. Educ.* **1959**, *36*, 3.

(29)   Davison, A.; Trop, H.; DePamphilis, B.; Jones, A. *Inorganic Synthesis* **1982**, *21*, 160.

(30)   Contant, R. *Inorg. Synth.* **1990**, *27*, 71.

(31)   Newville, M. *J. Synchrotron Rad.* **2001**, *8*, 322.

(32)   Ravel, B. *Physica Scripta* **2005**, *T115*, 1007.

(33)   Rehr, J. J.; Albers, R. C.; Zabinsky, S. I. *Phys. Rev. Lett.* **1992**, *69*, 3397.

(34)   D'Amour, V. H. *Acta Cryst.* **1976**, *B32*, 729.

(35)   Bevington, P. R.; Robinson, K. D. *Data Reduction and Error Analysis for the Physical Sciences*; McGraw-Hill: Boston, MA, 1992.

(36)   Downward, L.; Booth, C. H.; Lukens, W. W.; Bridges, F. In *AIP Conference Proceedings* 2007; Vol. 882, p 129.

(37)   Keita, B.; Girard, F.; Nadjo, L.; Contant, R.; Belghiche, R.; Abessi, M. *J. Electroanal. Chem.* **2001**, *508*, 70.

(38)   DePamphilis, B. V.; Jones, A. G.; Davison, A. *Inorg. Chem.* **1983**, *22*, 2292.

(39)   Davison, A.; DePamphilis, B. V.; Jones, A. G.; Franklin, K. L.; Lock, C. J. L. *Inorg. Chim. Acta* **1987**, *128*, 161.

(40)   Bonchio, M.; Bortolini, O.; Conte, V.; Sartorel, A. *Eur. Jour. Inorg. Chem.* **2003**, *4*, 699.

(41)   Deery, M. J.; Howarth, O. W.; Jennings, K. R. *J. Chem. Soc., Dalton Trans.* **1997**, 4783.

(42)   Finke, R. G.; Droege, M. W.; Domaille, P. J. *Inorg. Chem.* **1987**, *26*, 3886.

(43)   Finke, R. G.; Lyon, D. K.; Nomiya, K.; Sur, S.; Mizuno, N. *Inorg. Chem.* **1990**, *29*, 1784.

(44)   Finke, R. G.; Rapko, B.; Saxton, R. J.; Domaille, P. J. *J. Am. Chem. Soc.* **1986**, *108*, 2947.

(45)   Bartis, J.; Kunina, Y.; Blumenstein, M.; Francesconi, L. C. *Inorg. Chem.* **1996**, *35*, 1497.

(46)   Jorris, T. L.; Kozik, M.; Casan-Pastor, N.; Domaille, P. J.; Finke, R. G.; Miller, W. K.; Baker, L. C. W. *J. Am. Chem. Soc.* **1987**, *109*, 7402.

(47)   Bartis, J.; Dankova, M.; Lessmann, J. J.; Luo, Q.-H.; Horrocks, W. D., Jr.; Francesconi, L. C. *Inorganic Chemistry* **1999**, *38*, 1042.

(48)   Bartis, J.; Sukal, s.; Dankova, M.; Kraft, E.; Kronzon, R.; Blumenstein, M.; Francesconi, L. C. *J. Chem. Soc., Dalton Trans* **1997**, 1937.

(49)   Howell, R. C.; Perez, F. G.; Jain, S.; Horrocks, W. D., Jr.; Rheingold, A. L.; Francesconi, L. C. *Angew. Chem. Int. Ed.* **2001**, *40*, 4301.

(50)   Salmonte, J. L.; Pope, M. T. *Canadian Journal of Chemistry* **2001**, *79*, 802.

(51)   Zhang, C.; Bensaid, L.; McGregor, D.; Fang, X.; Howell, R. C.; Burton-Pye, B.; Q., L.; Todaro, L.; Francesconi, L. C. *Journal of Cluster Science* **2006**, *17*, 389.

(52)   Zhang, C.; Howell, R. C.; Scotland, K. B.; Perez, F. G.; Todaro, L.; Francesconi, L. C. *Inorg. Chem.* **2004**, *43*, 7691.

(53)   Keita, B.; Mbomekalle, I.-M.; Nadjo, L.; Contant, R. *Eur. J. Inorg. Chem.* **2002**, 473.

(54)   Acerete, R.; Hammer, C. F.; Baker, L. C. W. *Journ. Amer. Chem. Soc.* **1982**, *104*, 5384.

(55)   Dawson, B. *Acta. Cryst.* **1953**, *6*.

(56)   Kazansky, L. P.; Yamase, T. *J. Phys. Chem. A.* **2004**, *180*, 6437.

(57)   Tézé, A.; Canny, J.; Gurban, L.; Thouvenot, R.; Hervé, G. *Inorg Chem* **1996**, *35*, 1001.

(58)   Duncan, D. C.; Hill, C. L. *Inorg Chem* **1996**, *35*, 5828.

(59)   Kozik, M.; Hammer, C. F.; Baker, L. C. W. *J. Am. Chem. Soc.* **1986**, *108*, 2748.

(60)   Tézé, A.; Cadot, E.; Béreau, V.; Hervé, G. *Inorg Chem* **2001**, *40*, 2000.

(61)   Burke, I. T.; Boothman, C.; Lloyd, J. R.; Livens, F. R.; Charnock, J. M.; McBeth, J. M.; Mortimer, R. J. G.; Morris, K. *Environ. Sci. Technol.* **2006**, *ASAP article*.

(62)   Burke, I. T.; Boothman, C.; Lloyd, J. R.; Mortimer, R. J. G.; Livens, F. R.; Morris, K. *Environ. Sci. Technol.* **2005**, *39*, 4109.

(63)   Istok, J. D.; Senko, J. M.; Krumholz, L. R.; Watson, D.; Bogle, M. A.; Peacock, A.; Chang, Y. J.; White, D. C. *Environ. Sci. Technol.* **2004**, *38*, 468.

(64)   Lloyd, J. R.; Sole, V. A.; Van Praagh, C. V. G.; Lovley, D. R. *Appl. Environ. Microbiol.* **2000**, *66*, 3743.

(65)   Lukens, J., W.W.; Bucher, J. J.; Edelstein, N. M.; Shuh, D. K. *Environ. Sci. Technol.* **2002**, *36*, 1124.

(66)   Lukens, W. W.; Bucher, J. J.; Shuh, D. K.; Edelstein, N. M. *Environ. Sci. Technol.* **2005**, *39*, 8064.

(67)   Wildung, R. E.; Li, S. W.; Murray, C. J.; Krupka, K. M.; Xie, Y.; Hess, N. J.; Roden, E. E. *FEMS Microbiology Ecology* **2004**, *49*, 151.

(68)   Keita, B.; Belhouari, A.; Nadjo, L.; Contant, R. *J. Electroanal. Chem.* **1998**, *442*, 49.

(69)   Lopez, X.; Bo, C.; Poblet, J. M. *J. Amer. Chem. Soc.* **2002**, *124*, 12574.